To stabilize neutrophil polarity, PIP3 and Cdc42 augment RhoA activity at the back as well as signals at the front

Alexandra Van Keymeulen,[1,2,3] Kit Wong,[1,2,3] Zachary A. Knight,[1,2,3] Cedric Govaerts,[1,2,3] Klaus M. Hahn,[4,5] Kevan M. Shokat,[1,2,3] and Henry R. Bourne[1,2,3]

[1]Department of Cellular and Molecular Pharmacology, [2]Department of Medicine, and [3]Cardiovascular Research Institute, University of California, San Francisco, San Francisco, CA 94143
[4]Department of Pharmacology and [5]Lineberger Comprehensive Cancer Center, University of North Carolina, Chapel Hill, NC 27599

Chemoattractants like f-Met-Leu-Phe (fMLP) induce neutrophils to polarize by triggering divergent signals that promote the formation of protrusive filamentous actin (F-actin; frontness) and RhoA-dependent actomyosin contraction (backness). Frontness locally inhibits backness and vice versa. In neutrophil-like HL60 cells, blocking phosphatidylinositol-3,4,5-tris-phosphate (PIP3) accumulation with selective inhibitors of PIP3 synthesis completely prevents fMLP from activating a PIP3-dependent kinase and Cdc42 but not from stimulating F-actin accumulation. PIP3-deficient cells show reduced fMLP-dependent Rac activity and unstable pseudopods, which is consistent with the established role of PIP3 as a mediator of positive feedback pathways that augment Rac activation at the front. Surprisingly, such cells also show reduced RhoA activation and RhoA-dependent contraction at the trailing edge, leading to the formation of multiple lateral pseudopods. Cdc42 mediates PIP3's positive effect on RhoA activity. Thus, PIP3 and Cdc42 maintain stable polarity with a single front and a single back not only by strengthening pseudopods but also, at longer range, by promoting RhoA-dependent actomyosin contraction at the trailing edge.

Introduction

Polarity, an essential property of eukaryotic cells, allows yeast cells to bud and mate, epithelial cells to form apical and basolateral surfaces, neurons to form synapses, fibroblasts to heal wounds, and leukocytes to crawl to sites of infection. These behaviors require the orientation of polarity toward external cues that are detected by cell surface receptors, which trigger a complex interplay between Rho GTPases and the actin and microtubule cytoskeletons. At the cell's leading edge, this interplay often depends on phosphatidylinositol-3,4,5-tris-phosphate (PIP3), a membrane lipid, and creates positive feedback loops (Weiner et al., 2000; Devreotes and Janetopoulos, 2003).

A. Van Keymeulen and K. Wong contributed equally to this paper.

Correspondence to Henry R. Bourne: bourne@cmp.ucsf.edu

In differentiated HL60 (dHL60) cells, a neutrophil-like cell line, polarity is mediated by two divergent and competing sets of signals, both triggered by a single species of receptor (Xu et al., 2003). A tripeptide chemoattractant, f-Met-Leu-Phe (fMLP), triggers frontness (protrusive filamentous actin [F-actin] in pseudopods) by stimulating receptor-mediated activation of a trimeric G protein, Gi, which in turn initiates a signaling cascade in which positive feedback loops linking PIP3, Rac, and F-actin create robust pseudopods (Niggli, 2000; Wang et al., 2002; Weiner et al., 2002). fMLP stimulates backness (contractile actomyosin) by inducing the receptor-dependent activation of G12 and G13, which promote the activity of RhoA, a Rho-dependent kinase (p160–Rho-associated coil-containing protein kinase [ROCK]), and myosin II (Xu et al., 2003). In a polarized cell, RhoA-dependent backness confines frontness to pseudopods (Xu et al., 2003), whereas Rac-dependent frontness reciprocally constrains backness to the cell's trailing edge (Wong et al., 2006).

The ability of frontness and backness to inhibit one another locally helps to explain the segregation of these two responses in a polarized cell. However, it does not explain how uniformly

Supplemental Material can be found at:
http://www.jcb.org/cgi/content/full/jcb.200604113/DC1

applied fMLP elicits the formation of a single stable front rather than many in the absence of any spatial cue. Formation of a single stable front is similarly elicited by applying a uniform stimulus to many other cells: yeast, neurons, and *Dictyostelium discoideum* amoebae form one shmoo tip (Wedlich-Soldner et al., 2004), one axon (de Anda et al., 2005), or one pseudopod (Weiner et al., 2000; Devreotes and Janetopoulos, 2003), respectively.

In this study, we report that fMLP cannot elicit the formation of a single stable pseudopod in dHL60 cells treated with isoform-selective inhibitors of phosphatidylinositol 3′-kinases (PI3Ks). Inhibition of PI3Ks causes these cells to form pseudopods that are multiple, weak, and transient, leading to the loss of persistent migration and impaired chemotaxis. We also show that PIP3 stabilizes polarity in two ways: first, by locally enhancing Rac activity to stabilize frontness at the leading edge; and second, by stimulating the activation of Cdc42, which promotes RhoA-dependent backness at the trailing edge, thereby preventing the formation of multiple pseudopods.

Results

Effects of selective PI3K inhibition

To explore the roles of PIP3 in controlling polarity and chemotaxis, we assessed the effects of compounds that inhibit different subsets of four class I PI3K isoforms expressed in dHL60 cells (Vanhaesebroeck et al., 1997; Naccache et al., 2000; Sawyer et al., 2003; and unpublished data). From a wide range of PI3K-inhibiting compounds, we chose five that show distinct patterns of isoform selectivity (Table S1, available at http://www.jcb.org/cgi/content/full/jcb.200604113/DC1) in vitro (Knight et al., 2004, 2006): IC87114 (selectively inhibits δ), TGX-115 (β and δ), PI-103 (α > β and δ), PIK-90 (α, γ, and δ), and PIK-93 (α and γ > δ). None of the five compounds is excluded from intact dHL60 cells (supplemental Results), and all are more potent and selective than classical PI3K inhibitors (Knight et al., 2006). Of these compounds, PIK-90 and -93 are unique in their potencies for inhibiting PI3Kγ in vitro (Table S1), for completely inhibiting the fMLP-stimulated phosphorylation of Akt, a kinase downstream of PIP3 (phosphorylated Akt [pAkt]; Fig. S1 and Table S2), for preventing the accumulation in pseudopods of the fluorescent PIP3 probe pleckstrin homology domain (PH)–Akt-YFP (Fig. S2 A), and for impairing polarity and chemotaxis (Fig. 1). These results are consistent with observations (Hirsch et al., 2000; Li et al., 2000; Sasaki et al., 2000) in PI3Kγ knockout mice. Consequently, we used these two inhibitors to effectively inhibit PI3Kγ, although contributions from other isoforms to these responses cannot be completely ruled out (supplemental Results).

Treatment of dHL60 cells with PIK-90 or -93 impairs consolidation and stability of the leading edge formed after treatment with uniform fMLP, whereas the other three compounds do not (Fig. 1). None of the compounds significantly reduces the fMLP-dependent accumulation of total F-actin (Fig. S2 B), but PI3Kγ inhibition by treatment with PIK-90 or -93 alters its localization, as shown by the multiple pseudopods in Fig. 1 A. Multiple F-actin–containing pseudopods are twice as frequent in PIK-90– or -93–treated cells 3 min after exposure to uniform
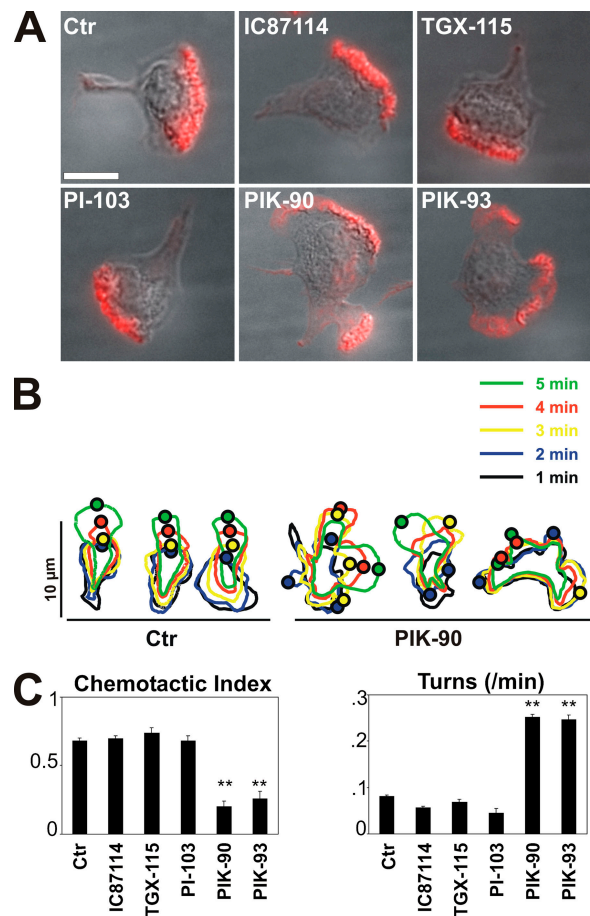

Figure 1. **Effects of PI3K inhibitors on polarity and chemotaxis.** (A) Cellular distribution of F-actin. Cells in suspension were exposed for 40 min either to no drugs, to 10 μM IC87114 or TGX-115, or to 1 μM PI-103, PIK-90, and PIK-93, allowed to stick to coverslips for 15 min, and treated with 100 nM fMLP for 3 min before fixation and staining for F-actin (red), as described in Materials and methods. Fluorescent and differential interference contrast images are merged. (Note that fMLP induced the formation of more than one leading edge in the individual cells shown for PIK-90 and -93, but this effect was not seen in all cells; see Results and Table S3) Bar, 10 μm. (B) Outlines of cells responding to stimulation with a uniform concentration of 100 nM fMLP. Cells were treated with or without 1 μM PIK-90 before treatment with fMLP. Each set of outlines represents a single cell observed at 1-min intervals (denoted by colors as indicated) after exposure to fMLP. Each small circle represents the center of a protruding lamellum at the periphery of each cell at the indicated time. Outlines on the left or right represent three control (Ctr) or three PIK-90–treated cells, respectively. Time-lapse videos of representative control or PIK-90–treated cells are shown in the supplemental material (Videos 1 and 2, respectively). (C) CI (left) and turning frequency of cells treated with the compounds indicated. Each bar represents the mean + one SEM (error bars) of different numbers of cells that were tested in multiple experiments: 30 control cells and 20, 10, 10, 29, and 18 cells for the compounds IC87114, TGX-115, PI-103, PIK-90, and PIK-93, respectively; concentrations of the same compounds were 10, 10, 0.5, 0.5, and 0.5 μm, respectively. Asterisks indicate that the value for cells treated with the compound differs from the corresponding control by P < 0.001. Trajectories of chemotaxing cells treated with two of these inhibitors are shown in Fig. S2 C (available at http://www.jcb.org/cgi/content/full/jcb.200604113/DC1).

fMLP relative to control cells or cells treated with the three other compounds (Table S3, available at http://www.jcb.org/cgi/content/full/jcb.200604113/DC1). Time-lapse microscopy (Fig. 1 B) revealed that PIK-90 treatment destabilizes pseudopods of living cells exposed to uniform fMLP. Control cells
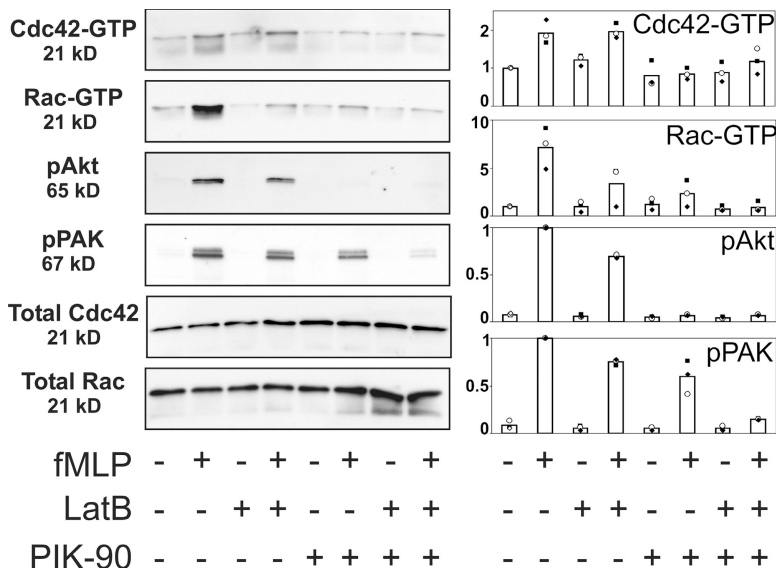
Figure 2. **Effects of PIK-90 and LatB on the fMLP-stimulated activities of Rac and Cdc42 and the phosphorylation of Akt and PAK.** Cells received no pretreatment or were exposed for 40 min to 40 µg/ml LatB, 0.5 µM PIK-90, or both and were stimulated with 100 nM fMLP for 1 min as indicated. Incubations were terminated, and lysates were prepared as indicated in Materials and methods. Rac-GTP (isoforms 1 and 2) and Cdc42-GTP were assessed by a GST-PAK-PBD pull-down assay; total Rac, pAkt, and pPAK were measured by immunoblotting aliquots of the lysate used for the pull-down reaction (see Materials and methods). The left panel shows representative blots for each condition. The right panel shows quantification of the immunoblots, which were measured with the Image program (Scion). The y axis represents immunoblot intensities (arbitrary scales). For each immunoblot, the background signal was subtracted and all values were normalized: for Cdc42-GTP and Rac-GTP, values were normalized to the signal (=1.0) detected in the absence of fMLP or inhibitor; and for pAkt and pPAK, values were normalized to the fMLP-dependent signal (=1.0) detected in the absence of inhibitor. Each graph represents the mean of three independent experiments, with different symbols representing the three actual values. Total Cdc42 and Rac in these extracts, which were not affected by PIK-90 or LatB, were used to check for equal loading in the different lanes.

(Fig. 1 B, left) typically polarize, form a single pseudopod, and crawl efficiently in one direction for several minutes; in contrast, the leading edges of PIK-90–treated cells (Fig. 1 B, right) persist for a short time (1–2 min) and retract, to be replaced by a leading edge at another site (Videos 1 and 2). Consequently, unlike control cells stimulated with uniform fMLP, PIK-90–treated cells fail to migrate persistently in one direction.

In fMLP gradients, PIK-90 and -93 substantially reduce the chemotactic index (CI; the ratio of a cell's displacement in the correct direction to the actual length of its migration path), whereas inhibitors selective for other PI3K isoforms do not (Fig. 1 C). In addition, PI3Kγ inhibition by either PIK-90 or -93 triples the cells' turning frequency, but the other three inhibitors have no effect (Fig. 1 C). PIK-90–treated cells migrate in jerky trajectories that are marked by frequent turns and less persistent orientation toward the source of attractant, which is in contrast to the straighter paths of control cells or cells treated with IC87114 (Fig. S2 C). Nonetheless, the PIK-90–treated cells interpret the fMLP gradient correctly in that their wavering trajectories accomplish net migration in the up-gradient direction (Fig. S2 C).

These results differ from our previous observations (Wang et al., 2002) with LY294002 or wortmannin in that dHL60 cells treated with either of these nonselective PI3K inhibitors showed poorly developed pseudopods and moved hardly at all (Wang et al., 2002). We suspect that this difference reflects the reported inhibition by the two nonselective agents of lipid and protein kinases that are distinct from PI3Ks (supplemental Results; Knight et al., 2006).

Frontness signals

Using pull-down assays or immunoblots of extracts of fMLP-treated cells (Fig. 2), we asked how frontness signals are affected by PIK-90 and latrunculin B (LatB), a toxin that blocks the formation of actin polymers by sequestering monomeric actin (Spector et al., 1983). LatB strongly reduces the fMLP-dependent accumulation of Rac-GTP and modestly reduces activation of the Rac- and Cdc42-dependent kinase p21-

activated kinase (PAK), which is assessed by the accumulation of phosphorylated PAK (pPAK). LatB modestly reduces fMLP-dependent pAkt accumulation as described previously (Wang et al., 2002) but has no effect on the accumulation of Cdc42-GTP. These effects presumably reflect the interruption of F-actin's participation in the PIP3–Rac–F-actin–dependent feedback loop in pseudopods (Niggli, 2000; Wang et al., 2002; Weiner et al., 2002) and suggest that Cdc42 activation is not subject to that feedback. Note that Fig. 2 shows results at a single time point (1 min); careful time course analysis showed that all four responses (Cdc42-GTP, Rac-GTP, pAkt, and pPAK) peak at 1 min in control cells and in cells treated with LatB or PIK-90 (not depicted).

Effects of PIK-90 (Fig. 2) show a different pattern: the complete inhibition of fMLP-dependent pAkt and Cdc42-GTP accumulation, modest inhibition of pPAK accumulation, and severe inhibition of Rac activation. We suspect that the small residual Rac activation seen in PIK-90–treated cells suffices to account for the fMLP-dependent elevation of normal amounts of F-actin (Fig. S2 B) and the formation of transient but multiple fMLP-stimulated pseudopods (Fig. 1, A and B; and Table S3). In keeping with this idea, the expression of the dominant-negative Rac mutant (Rac-N17) inhibits pseudopod formation in PIK-90–treated cells (Fig. 3 A). This result, of course, does not completely rule out a Rac-independent contribution to pseudopod formation because the Rac mutant could affect mechanisms that are distinct from the activation of endogenous Rac. Consistent with the observed modest inhibition of pPAK, the p21-binding domain (PBD) of PAK fused to CFP (PAK-PBD-CFP) still translocates to the periphery of PIK-90–treated cells that are treated with fMLP (Fig. 3 B). This probe was shown previously to reflect the localization of activated Rac in dHL60 (Srinivasan et al., 2003). Fig. 3 B shows that fMLP stimulates translocation of PAK-PBD-CFP to the entire cell periphery at 1 min of PIK-90–treated cells, whereas at 3 min, the probe accumulates at multiple sites, which correspond to multiple leading edges. The same is true of cells in which
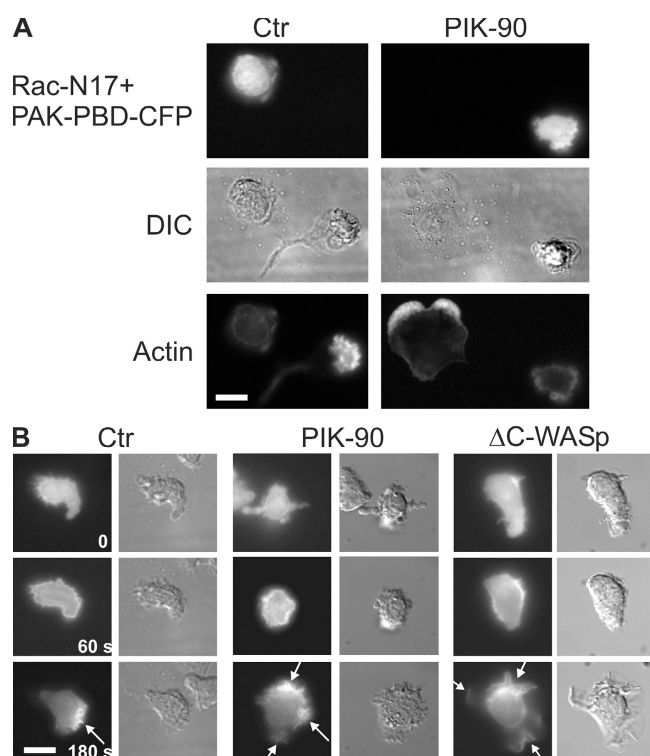
A

B

Figure 3. **Effects of PIK-90 and Cdc42 inhibition on the localization of Rac activity in pseudopods.** (A) Cellular distribution of F-actin in Rac-N17–expressing cells. Cells transiently coexpressing Rac-N17 and PAK-PBD-CFP were exposed for 40 min to no drugs or 1 μM PIK-90, allowed to stick to coverslips for 15 min, and treated with 100 nM fMLP for 3 min before fixation and staining for F-actin, as described in Materials and methods. Each set of pictures shows one cell expressing the fluorescent marker and one untransfected cell. (B) Cells expressing PAK-PBD-CFP pretreated in suspension with or without 1 μM PIK-90 for 40 min or cells coexpressing PAK-PBD-CFP and ΔC-WASp were allowed to stick to a coverslip for 15 min and were exposed to a uniform concentration of 100 nM fMLP. Images show the time course of response of a single control, a PIK-90–treated cell, and a ΔC-WASp–expressing cell at the times indicated after the addition of fMLP. Arrows point to pseudopods. Bars, 10 μm.

Cdc42 signals downstream of Cdc42-GTP are inhibited by the expression of ΔC-WASp.

Combined treatment with PIK-90 and LatB reduces the activation of both Rac and PAK to virtually nil (Fig. 2). Compared with the effects of the two treatments alone, the reduction of pPAK accumulation caused by the combination of inhibitors is very much greater, suggesting that separate pathways dependent on PIP3 and F-actin normally converge to stimulate the maximal activation of PAK. With respect to the accumulation of Rac-GTP, each treatment substantially reduces the fMLP response, but the two together appear to induce even greater inhibition.

PI3Kγ inhibition, Cdc42, and RhoA activity

fMLP promotes RhoA activation by a pathway that requires PIP3 and the activation of Cdc42 (Fig. 4). fMLP treatment of intact neutrophils induces RhoA to associate with the particulate fraction of extracts from these cells (Niggli, 2003); PIK-90 treatment reduces the basal RhoA content of particulate fractions and prevents the response to fMLP (Fig. 4 A). The same effects are seen with a second assay (Fig. 4 B) that is based on

the quantitative assessment of fluorescence resonance energy transfer (FRET) signals triggered by GTP occupying the guanine nucleotide-binding pocket of a recombinant RhoA biosensor (Pertz et al., 2006). As we previously reported (Wong et al., 2006), fMLP increases RhoA FRET in dHL60 cells. PIK-90 lowers basal RhoA FRET and prevents fMLP from elevating it (Fig. 4 B). (For representative RhoA FRET images of individual cells corresponding to the averaged values shown in Fig. 4 [B–G], see Fig. S3; available at http://www.jcb.org/cgi/content/full/jcb.200604113/DC1). In contrast, we previously reported (Xu et al., 2003) that LY294002 appeared to increase basal RhoA activity. This effect may reflect the documented (Knight et al., 2006) effects of LY294002 on kinases other than PI3Ks (for further discussion, see supplemental Results).

PIK-90 treatment prevents the fMLP-dependent activation of Cdc42 (Fig. 2), and Cdc42-GTP mediates RhoA activation in response to fMLP (Fig. 4, C and D). Expression of a constitutively active Cdc42 mutant, Cdc42-V12, significantly increases the mean RhoA FRET of cells that were not exposed to fMLP (Fig. 4 C). In addition, the expression of ΔC-WASp prevents fMLP from elevating the RhoA FRET signal (Fig. 4 D).

In addition to increasing RhoA activity (Fig. 4 C), Cdc42-V12 in dHL60 cells prevents fMLP from inducing ruffling and pseudopod formation, as previously described (Srinivasan et al., 2003) and confirmed in Fig. 5. In retrospect, we overlooked the potential importance of this surprising Cdc42 effect, which differs strikingly from the Cdc42-stimulated formation of the filopodia seen in fibroblasts (Welch and Mullins, 2002). Now we find that Cdc42-V12 inhibits ruffling and pseudopod formation because it induces the activation of a RhoA-dependent pathway that inhibits frontness responses. Indeed, morphologic effects of Cdc42-V12 are reversed by treating cells with Y27632 to inhibit p160-ROCK (Fig. 5), a kinase that links RhoA to the phosphorylation of myosin light chains and actomyosin contraction. Although only 1/10 Cdc42-V12–expressing cells made ruffles all around the cell at 1 min and formed an F-actin–containing leading edge at 3 min in response to fMLP, 9/11 cells expressing the mutant protein did so after exposure to Y27632 (unpublished data). The morphologic effect of constitutively active Cdc42 (Fig. 5) closely mimics the reported (Xu et al., 2003) effect of constitutively active RhoA, which was also reversed by exposure to Y27632.

Inhibiting Cdc42 with ΔC-WASp has an effect opposite to that of Cdc42-V12; that is, like PIK-90 and -93, it reduces fMLP-stimulated RhoA activity (Fig. 4 D). This inhibition of RhoA is paralleled by effects on fMLP-stimulated polarity and chemotaxis, which also resemble effects of the PI3K inhibitors. We reported previously (Srinivasan et al., 2003) that dominant-negative Cdc42 (Cdc42-N17) or ΔC-WASp cause cells to form multiple transient pseudopods in response to fMLP (Fig. 3 B). In the course of this study, we repeated these experiments and obtained virtually identical results (unpublished data). In addition, Cdc42-N17–expressing cells migrated toward an fMLP-containing micropipette in jerky trajectories marked by multiple turns (unpublished data); these trajectories closely resembled those of cells treated with PIK-90 (Fig. S2 C). We infer from these results that the fMLP-dependent activation of Cdc42, like the accumulation of PIP3, normally stimulates backness signals.
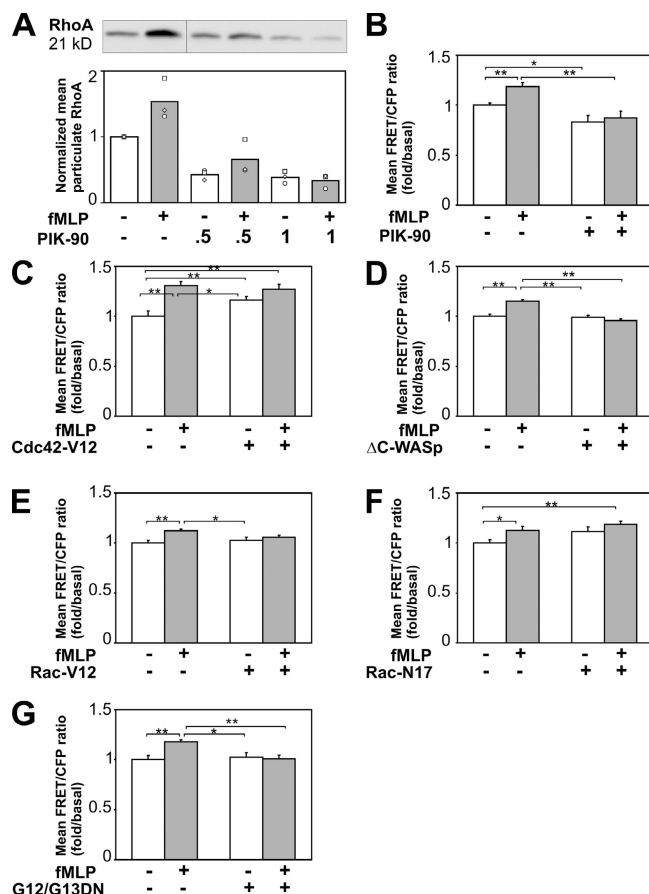
Figure 4. **RhoA activation depends on PI3Kγ and Cdc42.** (A) fMLP-induced membrane association of RhoA. Cells received no pretreatment or were exposed for 40 min to 0.5 or 1 μM of PIK-90 as indicated and were stimulated with or without 100 nM fMLP for 1 min as indicated. RhoA that associated with the particulate fraction of cell extracts was then assessed as described in Materials and methods. The top and bottom panels show a representative immunoblot and quantification of immunoblotted bands measured with the Image program (Scion), respectively. For each immunoblot, the background signal was subtracted, and the level of RhoA was normalized to that of transferrin in the particulate fraction; all values were further normalized to the signal detected in the absence of inhibitor, which was set at 1.0. Each graph represents the mean of three independent experiments, with different symbols representing the three actual values. (B–G) Quantification of mean FRET/CFP ratios in cells treated under different conditions. Data were obtained from n ≥ 25, 14, 18, 12, 13, or 13 cells in B–G, respectively, and were normalized to the FRET/CFP signal measured in unstimulated control cells. Similar results were observed in three independent experiments. Error bars indicate one SEM. t tests were performed to compare data of unstimulated control versus other experimental groups and between stimulated control and other conditions. Pairs of treatments that showed a statistically significant difference are marked with asterisks (*, P ≤ 0.05; **, P ≤ 0.001 by t test). (B) Lentivirus-transformed cells expressing the RhoA biosensor were treated with or without 1 μM PIK-90 for 40 min, stimulated with 100 nM fMLP for 3 min as indicated, fixed, and subjected to FRET imaging. (C–G) dHL60 cells transiently transfected with the RhoA biosensor and Cdc42-V12, ΔC-WASp, Rac-V12, Rac-N17, or G12/G12-DN, as indicated, were stimulated with 100 nM fMLP for 3 min as indicated.

Figure 5. **Treatment with the ROCK inhibitor Y27632 partially rescues the Cdc42-V12 phenotype.** Cells were transiently transfected with YFP-actin alone (control) or YFP-actin plus Cdc42-V12. After 4 h, cells were allowed to adhere to the coverslip in the presence of 10 μM Y27632 (for 20 min). Differential interference contrast and the corresponding fluorescent images are shown. Cells were then uniformly stimulated with 100 nM fMLP. Time after fMLP addition is indicated. Arrows point to pseudopods. Bar, 10 μm.

Because the loss of fMLP-dependent RhoA activation in PIK-90–treated cells is accompanied by the reduced activation of Rac (Fig. 2), we used Rac mutants to ask whether Rac-GTP plays a role in activating RhoA. Expression of a constitutively active Rac mutant, Rac-V12, failed to elevate RhoA biosensor
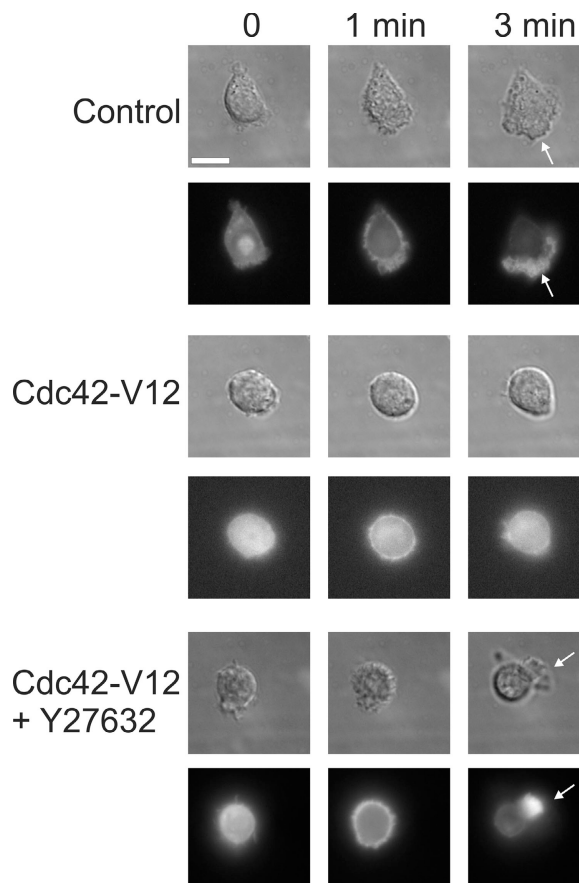
activity in unstimulated cells (Fig. 4 E), and Rac-N17, a dominant-negative mutant, did not inhibit the fMLP response (Fig. 4 F). These results are directly opposite to those seen with Cdc42-V12 and ΔC-WASp, respectively. We infer that Rac activation is neither sufficient nor necessary for RhoA activation.

Finally, we reported (Xu et al., 2003) that G12 and G13, which are trimeric G proteins, mediate fMLP stimulation of backness based on observations with constitutively active and dominant inhibitory mutants of these proteins. In accord with these findings, the expression of dominant-negative G12/13 prevents fMLP from activating the RhoA biosensor (Fig. 4 G). Because the multiple fMLP-dependent pseudopods of G12/13-inhibited cells accumulate prominent PH-Akt-GFP fluorescence (Xu et al., 2003), they presumably also accumulate PIP3 and Cdc42-GTP in response to fMLP, although such responses could not be quantitated. Therefore, we suspect that RhoA activation requires simultaneous positive inputs from G12/13 and the long-range pathway triggered by PIP3/Cdc42, although a strong Cdc42 signal (from Cdc42-V12) can override the requirement for G12/13. Cdc42 may also activate RhoA through G12/13 independently of the receptor, as suggested by the

increased basal RhoA activity in cells overexpressing a constitutively active Cdc42 in the absence of fMLP.

Discussion

Stabilizing broken symmetry

We proposed (Xu et al., 2003; Wong et al., 2006) that dHL60 cells polarize and break their symmetry when fMLP stimulates competing Gi-dependent frontness and G12/13-dependent backness responses whose mutual incompatibility causes them to segregate into separate membrane regions. However, breaking symmetry is not enough. Cells treated with PIK-90 or -93 break their symmetry in response to fMLP quite easily but do not maintain a single persistent pseudopod and a single persistent back; consequently, they cannot migrate persistently in one direction in uniform fMLP or migrate efficiently up fMLP gradients (Fig. 1). Intuitively, we might have suspected that competing frontness and backness responses alone would not suffice to maintain stable polarity. Responses of approximately equal strengths would probably produce a shifting array of multiple transient fronts and backs, whereas the excess strength of one response might easily enable it to win the competition. For instance, positive feedback loops between frontness signals could generate pseudopods covering the entire cell surface.

How, then, do neutrophils maintain stable polarity? Our experiments indicate that PIP3 and Cdc42, which were generated as part of the frontness response, exert a powerful stabilizing effect by strengthening pseudopods and by promoting long-range activation of Rho-dependent backness (Figs. 2 and 4). Inhibiting PI3Kγ or Cdc42 activity disrupts this stabilizing effect, leading to the formation of multiple transient pseudopods. Normally, however, PIP3 and Cdc42 signals originating in a strong pseudopod effectively promote G12/13- and RhoA-dependent actomyosin-based contractility at the cell's opposite end, and the proportionately stronger back increases the likelihood of achieving stable asymmetry with a single robust pseudopod and one back.

This scenario resembles local excitation global inhibition models (Meinhardt, 1999; Devreotes and Janetopoulos, 2003), which combine local positive feedback and a globally active diffusible inhibitor. For amoebae of *D. discoideum*, the local excitation global inhibition model (Devreotes and Janetopoulos, 2003; Janetopoulos et al., 2004) proposes that PIP3 at the front promotes actin polymerization with positive feedback, whereas an unidentified signal generates a rapidly diffusible mediator that activates phosphatase and tensin homologue (PTEN), a PIP3 phosphatase, at the back of the cell.

The Rho pathway is reported to enhance PTEN localization at the trailing edge of mouse neutrophils (Li et al., 2005). However, this effect is probably not essential for stabilizing neutrophil polarity because we (Xu et al., 2003) and others (Lacalle et al., 2004) could not detect PTEN localization to the trailing edge of dHL60 cells, and neither excess nor the depletion of PTEN altered gradient sensing (Lacalle et al., 2004).

Long-range effects of PIP3 and Cdc42

Just as actomyosin contraction constrains the pseudopod to a single location (Xu et al., 2003), local effects of protrusive F-actin at the front of the cell reciprocally inhibit RhoA activation and actomyosin-based contraction (Wong et al., 2006). How do PIP3 and Cdc42, which are generated at the leading edge, exert long-range positive regulation of RhoA outside pseudopods (Fig. 5)?

Long-range regulation involving PIP3 or Cdc42 has been described in other systems, but mechanisms are poorly understood. One precedent is the sharp segregation of Cdc42-GTP and RhoA-GTP into spatially separated concentric rings that surround and promote the closure of plasma membrane wounds in frog oocytes (Benink and Bement, 2005). Active Cdc42 in this system is physically separate from active RhoA but is nonetheless required for RhoA to become active. A second precedent is the ability of PIP3 at the leading edge of *D. discoideum* amoebae to trigger a kinase cascade that promotes myosin II contraction at the back (Chung et al., 2001). Instead of Cdc42 and Rho, the *D. discoideum* pathway depends on the PIP3-dependent activation of Akt/PKB and subsequent activation of PAKα, a PAK1 homologue located at the back of the cell. How the message moves from Akt/PKB at the front to PAKα at the back is unknown.

One possibility in dHL60 cells is that PIP3 and Cdc42 lead to the generation of a phosphorylated protein or a cytosolic second messenger that diffuses rapidly from the front to the back. The putative diffusible mediator could augment activation of a Rho guanine nucleotide exchange factor or inhibit activity of a GTPase-activating protein that inactivates Rho. Alternatively, Cdc42 could also promote transport of a regulator from front to back via endocytosed vesicles and microtubules. A possible role for microtubules is consistent with the documented ability of Cdc42 to regulate the interaction of microtubules with the cell cortex (Wittmann and Waterman-Storer, 2001; Gundersen, 2002), with microtubule-dependent delivery of a Rho guanine nucleotide exchange factor to the plasma membrane of *Drosophila melanogaster* S2 cells (Rogers et al., 2004), and with microtubule-dependent localization of RhoA activity at the cleavage plane of frog oocytes (Bement et al., 2005).

Cdc42 has been reported to regulate actomyosin contraction via myotonic dystrophy kinase-related Cdc42-binding kinase independently of ROCK (Wilkinson et al., 2005). Such a role for myotonic dystrophy kinase-related Cdc42-binding kinase is unlikely to be quantitatively important in fMLP-treated dHL60 cells because inhibiting ROCK with Y27632 rescues the inability of Cdc42-V12–expressing cells to form pseudopods (Fig. 5).

PIP3, Rac, and Cdc42 cooperate at the leading edge

Why are pseudopods of PIK-90–treated cells weak and transient (Fig. 1) despite the accumulation of quantitatively normal amounts of F-actin (Fig. S2 B)? The most likely explanation is that reduced PIP3 accumulation dramatically reduces the activation of Rac (Fig. 2), an essential positive regulator of actin polymerization. Our results also suggest that the loss of PIP3 inhibits the consolidation of Rac activity into one region of the cell periphery so that the remaining active Rac, which is detected by the localization of PAK-PBD-CFP, localizes in multiple transient pseudopods (Fig. 3 B).

Maintaining strong pseudopods may require positive PIP3-dependent signals mediated by Cd42 as well as Rac. Indeed, the pseudopod defects of cells exposed to PIK-90 and -93 inhibitors (Fig. 1) closely resemble those of cells expressing inhibitors of Cdc42 (Srinivasan et al., 2003): in both cases, pseudopods are not only multiple but are also transient and weak. One potential integrator of Rac and Cdc42 signals in pseudopods is PAK1, which can be activated by both GTPases, phosphorylates numerous cytoskeletal regulators, and promotes the formation of protrusive actin with the inhibition of contractile actomyosin (Bokoch, 2003). In favor of this possibility, PAK1 in dHL60 cells appears to be regulated by a PIP3-dependent signal in addition to an F-actin–dependent positive feedback signal; either PIK-90 or LatB treatment alone only inhibits a portion of the pPAK response, but inhibiting both signals blocks the response almost completely (Fig. 2). Finally, it is also possible that Cdc42 augments pseudopod strength and stability by stimulating actin polymerization directly via Wiskott-Aldrich Syndrome proteins (Welch and Mullins, 2002).

Conclusions

We have shown that PIP3 and Cdc42 in dHL60 cells stabilize polarity in two ways: by making pseudopods more robust and also by augmenting Rho-dependent actomyosin contraction at the trailing edge. Although initiated by signals generated at the front of the cell, the latter effect is manifested at the back of the cell as an augmentation of the fMLP- and G12/13-dependent activation of RhoA. This long-range activation of RhoA and the resulting actomyosin contraction serve to inhibit the formation of protrusive pseudopods, thereby maintaining robust polarity with a single pseudopod and a single back.

The present findings should stimulate further investigation in at least three directions. First, we need to understand the molecular mechanisms that connect Cdc42 to RhoA across the cell's diameter. Second, because inhibiting PIP3 accumulation and Cdc42 activation impairs but does not completely abolish dHL60 polarity and chemotaxis, polarity is probably supported by additional long-range interactions between signals generated at the front or back and reinforcing polarity responses at the opposite side of the cell. Finally, intuition must be converted into a model that quantitatively predicts the effects of perturbing specific signals on the initiation and stability of polarity.

Materials and methods

Materials

Antibodies against Akt, phosphorylated at T308 (pAkt) and PAK and phosphorylated at S199/204 (pPAK), were obtained from Cell Signaling Technology. Mouse monoclonal antibody against RhoA was purchased from Santa Cruz Biotechnology, Inc. Mouse antitransferrin receptor antibody was purchased from Zymed Laboratories. LatB and Y27632 were obtained from Calbiochem, and GST-PAK-PBD and antibodies against Rac (isoforms 1 and 2) were purchased from Pierce Chemical Co. Rhodamine-phalloidin was obtained from Invitrogen, and human fibronectin was obtained from BD Biosciences. Protease and phosphatase inhibitor cocktails and fMLP were obtained from Sigma-Aldrich. HRP-conjugated donkey anti–rabbit and anti–mouse IgG were purchased from GE Healthcare. Glass capillaries obtained from Frederick Haer Co. were converted into micropipettes with a puller (P-87; Sutter Instrument Co.). Compounds IC87114, TGX-115, PI-103, and PIK-93 were dissolved in DMSO; PIK-90 was dissolved in 50:50 DMSO/H_2O; all compounds were stored at

−20°C. Final dilutions were performed in cell media, with a final DMSO dilution of 0.5% for PIK-90 and 1.0% for the other compounds.

DNA constructs and lentiviral expression

Myc-tagged V12-Cdc42 cloned in pTET7 was described previously (Kalman et al., 1999a); to activate its expression, this construct was co-transfected with a plasmid constitutively expressing a tetracycline repressor VP16 fusion protein, as also described previously (Srinivasan et al., 2003). Myc-tagged Rac-V12 and Rac-N17 were purchased from the Guthrie cDNA Resource Center. ΔC-WASp (Kalman et al., 1999b) and PAK-PBD-CFP (Kraynov et al., 2000) were described previously. The RhoA biosensor construct used for transient transfection was described previously (Pertz et al., 2006). Quasi-stable expression of the RhoA biosensor or PH-Akt-YFP was accomplished by lentiviral transfection as described previously (Wong et al., 2006). G12- and G13-DN constructs (residues 326–379 for Gα12 and residues 321–377 for Gα13) were gifts from Y. Takuwa (Kanazawa University, Kanazawa, Japan) and were described previously (Sugimoto et al., 2003). Transient transfection with the RhoA biosensor, Cdc42-V12, ΔC-WASp, Rac-V12, Rac-N17, or G12/G13-DN was previously described (Srinivasan et al., 2003); experiments were performed 4 h after transfection.

Cell culture

Procedures for cultivation and DMSO-stimulated differentiation of HL60 cells have been previously described (Servant et al., 2000).

Microscopic analysis

Live dHL60 cells were imaged in 1.5% human albumin in modified HBSS (mHBSS) at room temperature using an inverted microscope (Eclipse TE200; Nikon) equipped with a Photometrics cooled CCD camera (CE300; Roper Scientific) driven by DeltaVision software (Applied Precision). Pictures shown were taken with a 60× NA 1.40 oil planApo objective (Nikon), whereas tracking experiments were performed with a 20× NA 0.75 planApo objective (Nikon). Cell trajectories were tracked using SoftWorx software (Applied Precision). The CI was calculated as described previously (Xu et al., 2005): CI = (AO − BO)/AB, where O is the position of the micropipette; A and B are the cell's position at time = 0 and time = 25 min, respectively; AO is the distance from A to O; BO is the distance from B to O; and AB is the actual length of the cell's curving migration path from HL60 A to B. Turns in a cell trajectory were quantified by approximating the cell's trajectory over successive 2-min intervals, with a vector derived from a least squares deviation fit to five successive positions of the leading edge (coordinates are assessed at 30-s intervals). Angles between each successive pair of vectors were computed; a turn was defined as a deviation of one 2-min vector from its predecessor by 60° or more in either direction.

Actin staining

dHL60 cells were preincubated in suspension with IC87114, TGX-115, PI-103, PIK-90, PIK-93, or no treatment for 40 min, centrifuged for 5 min at 2,000 rpm at room temperature in a J6-B centrifuge (Beckman Coulter), resuspended in mHBSS containing the respective agent at the same concentration, allowed to stick to fibronectin-covered coverslips, and subjected to stimulation with a uniform concentration of 100 nM fMLP for 3 min. Cells were fixed in 3.7% PFA and stained with 10 units/ml rhodamine-phalloidin for 15 min.

Pull-down assay for activated Cdc42 and Rac

dHL60 cells were preincubated for 40 min with 40 μg/ml LatB, 0.5 μM PIK-90, or both, centrifuged for 5 min at 2,000 rpm at room temperature in a J6-B centrifuge (Beckman Coulter), resuspended in mHBSS ($2 × 10^7$ cells in 0.5 ml per condition), and stimulated or unstimulated for 1 min with 100 nM fMLP. The reaction was stopped by adding 0.5 ml of 2× lysis buffer at 4°C (1× lysis buffer: 25 mM Tris-HCl, pH 7.5, 150 mM NaCl, 5 mM $MgCl_2$, 1% NP-40, 1 mM DTT, and 5% glycerol, protease inhibitor, and phosphatase inhibitor cocktails). Subsequent steps were performed as described in the protocol attached to the Cdc42 and Rac pull-down kit (Pierce Chemical Co.).

Assay for particulate-associated RhoA

dHL60 cells with or without 40 min of pretreatment with 0.5 or 1 μM PIK-90 were stimulated for 0 or 1 min with 100 nM fMLP. Particulate fractions were prepared as described previously (Xu et al., 2005). The level of RhoA in the particulate fraction was normalized to that of the transferrin receptor. This assay was first described by Niggli (2003). For comparison, the normalized data were further standardized by setting the unstimulated control value to one.

FRET analysis

Cells quasi-stably expressing the RhoA biosensor were pretreated with or without 1 μM PIK-90 for 40 min, resuspended in 1.5% human albumin in mHBSS, and plated on fibronectin-coated coverslips before treatment with or without 100 nM fMLP for 3 min. Cells transiently cotransfected with the RhoA biosensor and Cdc42-V12, ΔC-WASp, Rac-V12-myc, Rac-N17-myc, or G12 and G13 dominant-negative mutants were subjected to the same procedure without exposure to PIK-90. Images were acquired at room temperature, and data were processed as described previously (Wong et al., 2006).

Online supplemental material

Supplemental material provides details about the selectivity of PI3K inhibitors and methods for the F-actin. Table S1 provides IC50 values for inhibiting class I PI3K isoforms in vitro. Table S2 provides IC50 values of five compounds for inhibiting pAkt accumulation in dHL60 cells. Table S3 provides data on how PI3Kγ inhibitors induce cells to form multiple leading edges in response to fMLP. Fig. S1 shows the effects of five PI3K inhibitors on the phosphorylation of Akt in dHL60 cells. Fig. S2 shows the effects of inhibiting PI3Kγ on PIP3 localization, accumulation of F-actin, and chemotaxis. Fig. S3 shows the subcellular distribution of the FRET signal. Video 1 shows YFP-actin–expressing cells in uniform stimulation, and Video 2 shows PIK-90–treated YFP-actin–expressing cells in uniform stimulation. Online supplemental material is available at http://www.jcb.org/cgi/content/full/jcb.200604113/DC1.

References

Bement, W.M., H.A. Benink, and G. von Dassow. 2005. A microtubule-dependent zone of active RhoA during cleavage plane specification. *J. Cell Biol.* 170:91–101.

Benink, H.A., and W.M. Bement. 2005. Concentric zones of active RhoA and Cdc42 around single cell wounds. *J. Cell Biol.* 168:429–439.

Bokoch, G.M. 2003. Biology of the p21-activated kinases. *Annu. Rev. Biochem.* 72:743–781.

Chung, C.Y., G. Potikyan, and R.A. Firtel. 2001. Control of cell polarity and chemotaxis by Akt/PKB and PI3 kinase through the regulation of PAKa. *Mol. Cell.* 7:937–947.

de Anda, F.C., G. Pollarolo, J.S. Da Silva, P.G. Camoletto, F. Feiguin, and C.G. Dotti. 2005. Centrosome localization determines neuronal polarity. *Nature.* 436:704–708.

Devreotes, P., and C. Janetopoulos. 2003. Eukaryotic chemotaxis: distinctions between directional sensing and polarization. *J. Biol. Chem.* 278:20445–20448.

Gundersen, G.G. 2002. Microtubule capture: IQGAP and CLIP-170 expand the repertoire. *Curr. Biol.* 12:R645–R647.

Hirsch, E., V.L. Katanaev, C. Garlanda, O. Azzolino, L. Pirola, L. Silengo, S. Sozzani, A. Mantovani, F. Altruda, and M.P. Wymann. 2000. Central role for G protein-coupled phosphoinositide 3-kinase γ in inflammation. *Science.* 287:1049–1053.

Janetopoulos, C., L. Ma, P.N. Devreotes, and P.A. Iglesias. 2004. Chemoattractant-induced phosphatidylinositol 3,4,5-trisphosphate accumulation is spatially amplified and adapts, independent of the actin cytoskeleton. *Proc. Natl. Acad. Sci. USA.* 101:8951–8956.

Kalman, D., S.N. Gomperts, S. Hardy, M. Kitamura, and J.M. Bishop. 1999a. Ras family GTPases control growth of astrocyte processes. *Mol. Biol. Cell.* 10:1665–1683.

Kalman, D., O.D. Weiner, D.L. Goosney, J.W. Sedat, B.B. Finlay, A. Abo, and J.M. Bishop. 1999b. Enteropathogenic *E. coli* acts through WASP and Arp2/3 complex to form actin pedestals. *Nat. Cell Biol.* 1:389–391.

Knight, Z.A., G.G. Chiang, P.J. Alaimo, D.M. Kenski, C.B. Ho, K. Coan, R.T. Abraham, and K.M. Shokat. 2004. Isoform-specific phosphoinositide 3-kinase inhibitors from an arylmorpholine scaffold. *Bioorg. Med. Chem.* 12:4749–4759.

Knight, Z.A., B. Gonzalez, M.E. Feldman, E. Zunder, D.D. Goldenberg, O. Williams, R. Loweith, D. Stokoe, A. Balla, B. Toth, et al. 2006. A pharmacological map of the PI-K family defines a role for p110alpha in insulin signaling. *Cell.* 125:733–747.

Kraynov, V.S., C. Chamberlain, G.M. Bokoch, M.A. Schwartz, S. Slabaugh, and K.M. Hahn. 2000. Localized Rac activation dynamics visualized in living cells. *Science.* 290:333–337.

Lacalle, R.A., C. Gomez-Mouton, D.F. Barber, S. Jimenez-Baranda, E. Mira, A.C. Martinez, A.C. Carrera, and S. Manes. 2004. PTEN regulates motility but not directionality during leukocyte chemotaxis. *J. Cell Sci.* 117:6207–6215.

Li, Z., H. Jiang, W. Xie, Z. Zhang, A.V. Smrcka, and D. Wu. 2000. Roles of PLC-beta2 and -beta3 and PI3Kgamma in chemoattractant-mediated signal transduction. *Science.* 287:1046–1049.

Li, Z., X. Dong, Z. Wang, W. Liu, N. Deng, Y. Ding, L. Tang, T. Hla, R. Zeng, L. Li, and D. Wu. 2005. Regulation of PTEN by Rho small GTPases. *Nat. Cell Biol.* 7:399–404.

Meinhardt, H. 1999. Orientation of chemotactic cells and growth cones: models and mechanisms. *J. Cell Sci.* 112:2867–2874.

Naccache, P.H., S. Levasseur, G. Lachance, S. Chakravarti, S.G. Bourgoin, and S.R. McColl. 2000. Stimulation of human neutrophils by chemotactic factors is associated with the activation of phosphatidylinositol 3-kinase gamma. *J. Biol. Chem.* 275:23636–23641.

Niggli, V. 2000. A membrane-permeant ester of phosphatidylinositol 3,4,5-trisphosphate (PIP3) is an activator of human neutrophil migration. *FEBS Lett.* 473:217–221.

Niggli, V. 2003. Microtubule-disruption-induced and chemotactic-peptide-induced migration of human neutrophils: implications for differential sets of signalling pathways. *J. Cell Sci.* 116:813–822.

Pertz, O., L. Hodgson, R.L. Klemke, and K.M. Hahn. 2006. Spatiotemporal dynamics of RhoA activity in migrating cells. *Nature.* 440:1069–1072.

Rogers, S.L., U. Wiedemann, U. Hacker, C. Turck, and R.D. Vale. 2004. *Drosophila* RhoGEF2 associates with microtubule plus ends in an EB1-dependent manner. *Curr. Biol.* 14:1827–1833.

Sasaki, T., J. Irie-Sasaki, R.G. Jones, A.J. Oliveira-dos-Santos, W.L. Stanford, B. Bolon, A. Wakeham, A. Itie, D. Bouchard, I. Kozieradzki, et al. 2000. Function of PI3Kgamma in thymocyte development, T cell activation, and neutrophil migration. *Science.* 287:1040–1046.

Sawyer, C., J. Sturge, D.C. Bennett, M.J. O'Hare, W.E. Allen, J. Bain, G.E. Jones, and B. Vanhaesebroeck. 2003. Regulation of breast cancer cell chemotaxis by the phosphoinositide 3-kinase p110delta. *Cancer Res.* 63:1667–1675.

Servant, G., O.D. Weiner, P. Herzmark, T. Balla, J.W. Sedat, and H.R. Bourne. 2000. Polarization of chemoattractant receptor signaling during neutrophil chemotaxis. *Science.* 287:1037–1040.

Spector, I., N.R. Shochet, Y. Kashman, and A. Groweiss. 1983. Latrunculins: novel marine toxins that disrupt microfilament organization in cultured cells. *Science.* 219:493–495.

Srinivasan, S., F. Wang, S. Glavas, A. Ott, F. Hofmann, K. Aktories, D. Kalman, and H.R. Bourne. 2003. Rac and Cdc42 play distinct roles in regulating PI(3,4,5)P3 and polarity during neutrophil chemotaxis. *J. Cell Biol.* 160:375–385.

Sugimoto, N., N. Takuwa, H. Okamoto, S. Sakurada, and Y. Takuwa. 2003. Inhibitory and stimulatory regulation of Rac and cell motility by the G12/13-Rho and Gi pathways integrated downstream of a single G protein-coupled sphingosine-1-phosphate receptor isoform. *Mol. Cell. Biol.* 23:1534–1545.

Vanhaesebroeck, B., M.J. Welham, K. Kotani, R. Stein, P.H. Warne, M.J. Zvelebil, K. Higashi, S. Volinia, J. Downward, and M.D. Waterfield. 1997. P110delta, a novel phosphoinositide 3-kinase in leukocytes. *Proc. Natl. Acad. Sci. USA.* 94:4330–4335.

Wang, F., P. Herzmark, O.D. Weiner, S. Srinivasan, G. Servant, and H.R. Bourne. 2002. Lipid products of PI(3)Ks maintain persistent cell polarity and directed motility in neutrophils. *Nat. Cell Biol.* 4:513–518.

Wedlich-Soldner, R., S.C. Wai, T. Schmidt, and R. Li. 2004. Robust cell polarity is a dynamic state established by coupling transport and GTPase signaling. *J. Cell Biol.* 166:889–900.

Weiner, O.D., G. Servant, C.A. Parent, P.N. Devreotes, and H.R. Bourne. 2000. Cell polarity in response to chemoattractants. *In* Cell Polarity: Frontiers in Molecular Biology. D.G. Drubin, editor. Oxford University Press, New York. 201–239.

Weiner, O.D., P.O. Neilsen, G.D. Prestwich, M.W. Kirschner, L.C. Cantley, and H.R. Bourne. 2002. A PtdInsP(3)- and Rho GTPase-mediated positive feedback loop regulates neutrophil polarity. *Nat. Cell Biol.* 4:509–513.

Welch, M.D., and R.D. Mullins. 2002. Cellular control of actin nucleation. *Annu. Rev. Cell Dev. Biol.* 18:247–288.

Wilkinson, S., H.F. Paterson, and C.J. Marshall. 2005. Cdc42-MRCK and Rho-ROCK signalling cooperate in myosin phosphorylation and cell invasion. *Nat. Cell Biol.* 7:255–261.

Wittmann, T., and C.M. Waterman-Storer. 2001. Cell motility: can Rho GTPases and microtubules point the way? *J. Cell Sci.* 114:3795–3803.

Wong, K., O. Pertz, K. Hahn, and H. Bourne. 2006. Neutrophil polarization: spatiotemporal dynamics of RhoA activity support a self-organizing mechanism. *Proc. Natl. Acad. Sci. USA.* 103:3639–3644.

Xu, J., F. Wang, A. Van Keymeulen, P. Herzmark, A. Straight, K. Kelly, Y. Takuwa, N. Sugimoto, T. Mitchison, and H.R. Bourne. 2003. Divergent signals and cytoskeletal assemblies regulate self-organizing polarity in neutrophils. *Cell.* 114:201–214.

Xu, J., F. Wang, A. Van Keymeulen, M. Rentel, and H.R. Bourne. 2005. Neutrophil microtubules suppress polarity and enhance directional migration. *Proc. Natl. Acad. Sci. USA.* 102:6884–6889.